Journal of Experimental Botany, Vol. 70, No. 2 pp. 589–597, 2019
doi:10.1093/jxb/ery368 Advance Access publication 30 October 2018
This paper is available online free of all access charges (see http://jxb.oxfordjournals.org/open_access.html for further details)

RESEARCH PAPER

CO_2 modulation of the rates of photosynthesis and light-dependent O_2 consumption in *Trichodesmium*

Tobias G. Boatman[1,2,*], Phillip A. Davey[1], Tracy Lawson[1] and Richard J. Geider[1]

[1] School of Biological Sciences, University of Essex, Wivenhoe Park, Colchester CO4 3SQ, UK
[2] Department of Chemical Engineering, Imperial College London, South Kensington, London SW7 2AZ, UK

* Correspondence: t.boatman@imperial.ac.uk

Received 6 June 2018; Editorial decision 15 October 2018; Accepted 23 October 2018

Editor: Howard Griffiths, University of Cambridge, UK.

Abstract

As atmospheric CO_2 concentrations increase, so too does the dissolved CO_2 and HCO_3^- concentrations in the world's oceans. There are still many uncertainties regarding the biological response of key groups of organisms to these changing conditions, which is crucial for predicting future species distributions, primary productivity rates, and biogeochemical cycling. In this study, we established the relationship between gross photosynthetic O_2 evolution and light-dependent O_2 consumption in *Trichodesmium erythraeum* IMS101 acclimated to three targeted pCO_2 concentrations (180 µmol mol^{-1}=low-CO_2, 380 µmol mol^{-1}=mid-CO_2, and 720 µmol mol^{-1}=high-CO_2). We found that biomass- (carbon) specific, light-saturated maximum net O_2 evolution rates ($P_{nC,max}$) and acclimated growth rates increased from low- to mid-CO_2, but did not differ significantly between mid- and high-CO_2. Dark respiration rates were five times higher than required to maintain cellular metabolism, suggesting that respiration provides a substantial proportion of the ATP and reductant for N_2 fixation. Oxygen uptake increased linearly with gross O_2 evolution across light intensities ranging from darkness to 1100 µmol photons m^{-2} s^{-1}. The slope of this relationship decreased with increasing CO_2, which we attribute to the increased energetic cost of operating the carbon-concentrating mechanism at lower CO_2 concentrations. Our results indicate that net photosynthesis and growth of *T. erythraeum* IMS101 would have been severely CO_2 limited at the last glacial maximum, but that the direct effect of future increases of CO_2 may only cause marginal increases in growth.

Keywords: Carbon fixation, CO_2, cyanobacteria, gross photosynthesis, net photosynthesis, ocean acidification, *Trichodesmium*.

Introduction

The ocean is one of the largest readily exchangeable reservoirs of inorganic carbon on Earth and is a major sink for anthropogenic CO_2 emissions (Sabine *et al.*, 2004). The ocean's capacity to sequester atmospheric CO_2 is strongly mediated by biological processes (Raven and Falkowski, 1999), where organic matter production and export drive CO_2 sequestration. This is important as future emission scenarios predict that atmospheric CO_2 will increase from present concentrations (~400 µmol mol^{-1}) to 750 µmol mol^{-1} or 1000 µmol mol^{-1} by the end of this century (Raven *et al.*, 2005). This will lead to an increase in the total dissolved inorganic carbon (TIC) in the surface ocean, reducing the pH from an average value of ~8.2 (pre-industrial) to ~7.9 (estimated for 2100) (Zeebe *et al.*, 1999; Zeebe and Wolf-Gladrow, 2001). Ocean acidification therefore favours an increase in seawater CO_2 and HCO_3^- concentration and a decrease in pH and CO_3^{2-}.

There are still many uncertainties regarding the biological response of key groups of organisms to these changing conditions, which is crucial for predicting future species distributions, primary productivity rates, and biogeochemical cycling. One group of great importance are diazotrophic cyanobacteria (photosynthetic dinitrogen fixers), as they contribute significantly to overall marine primary productivity by providing new nitrogen to many oligotrophic areas of the oceans. The filamentous cyanobacteria *Trichodesmium* are a colony-forming species that forms extensive surface blooms in the tropical and subtropical oceans (Carpenter and Capone, 1992; Capone *et al.*, 1997; Campbell *et al.*, 2005). *Trichodesmium* plays a significant role in the N cycle of the oligotrophic oceans; fixing nitrogen in an area corresponding to half of the Earth's surface (Davis and McGillicuddy, 2006) and representing up to 50% of new production in some oligotrophic tropical and subtropical oceans (Capone, 2005). The annual marine N_2 fixation is currently estimated at between 100 Tg and 200 Tg N per year (Gruber and Sarmiento, 1997; Karl *et al.*, 2002), of which *Trichodesmium* spp. contribute between 80 Tg and 110 Tg of fixed N_2 to open ocean ecosystems (Capone *et al.*, 1997).

Cyanobacteria have performed oxygenic photosynthesis for ~2.7 billion years (Buick, 2008). During that time, CO_2 concentrations have declined and O_2 concentrations increased, thus exerting an evolutionary pressure to form a mechanism to reduce the impact of photorespiration on photosynthetic CO_2 fixation. Despite cyanobacterial Rubisco having a relatively low affinity for CO_2, cyanobacteria achieve high photosynthetic rates by virtue of an intracellular carbon-concentrating mechanism (CCM), which thereby reduces the diversion of energy into oxygenation of ribulose-1,5-bisphosphate (RuBP), the first step in photorespiration (Schwarz *et al.*, 1995; Kaplan and Reinhold, 1999). In addition, the CCM can aid in the dissipation of excess light energy as well as maintaining an optimal intracellular pH (Badger *et al.*, 1994; Kaplan and Reinhold, 1999).

Cyanobacteria have a unique ability to perform both photosynthesis and respiration simultaneously in the same cellular compartment (Nagarajan and Pakrasi, 2001). The thylakoid membranes of cyanobacteria contain both respiratory and photosynthetic electron transport chains, sharing the plastoquinone and plastocyanin pools and the Cyt b_6f complex. In contrast, the cytoplasmic membrane is only capable of performing respiratory electron transport (Nagarajan and Pakrasi, 2001). Thus, it is common in cyanobacteria for respiratory electron transport to be inhibited at low light intensities as photosynthesis increases in the thylakoid membranes (Kana, 1992). However, in *Trichodesmium* there remains the possibility that photosynthetic and respiratory metabolism differs between diazocytes (where N_2 fixation occurs) and other cells within a trichome.

Previous studies report an increase in growth and productivity (CO_2 and N_2 fixation) of *T. erythraeum* IMS101 as well as changing elemental composition in response to future CO_2 concentrations (~750–1000 μmol mol^{-1}) (Barcelos e Ramos *et al.*, 2007; Levitan *et al.*, 2007, 2010*a*; Kranz *et al.*, 2010; Spungin *et al.*, 2014; Hutchins *et al.*, 2015; Boatman *et al.*, 2017, 2018*a*, *b*), although, as discussed in Boatman *et al.* (2018*a*), the magnitude of the responses often differs between studies. Due to the significant contribution that *Trichodesmium* makes to biogeochemical cycles and the predicted change in inorganic carbon (Ci) speciation over the coming decades, we performed a systematic experiment to assess how the photosynthetic physiology of *T. erythraeum* IMS101 was affected by acclimation to varying CO_2. We ensured that the Ci chemistry and all other growth conditions were well defined, with cultures fully acclimated over long time periods (~5 months) to achieve balanced growth. We assessed the dark respiration, light absorption, and the light dependencies of gross O_2 evolution and O_2 consumption across different CO_2 conditions. We discuss how the responses that we observed may be related to N_2 fixation and changes in the cost of operating the CCM.

Materials and methods

Trichodesmium erythraeum IMS101 was semi-continuously cultured to achieve fully acclimated balanced growth at three target pCO_2 concentrations (180, 380, and 720 μmol mol^{-1}), under saturating light intensity (400 μmol photons m^{-2} s^{-1}), a 12/12 h light/dark (L/D) cycle, and an optimum growth temperature (26 ± 0.7 °C) for ~5 months (~40, 70, and 80 generations at low-, mid-, and high-CO_2, respectively).

Experimental set-up

Cultures of *T. erythraeum* IMS101 were grown in standard YBCII medium (Chen *et al.*, 1996) under diazotrophic conditions (N_2 only) in 1.5 litre volumes in 2 litre Pyrex bottles that had been acid-washed and autoclaved prior to culturing. Illumination was provided side-on by fluorescent tubes (Sylvania Luxline Plus FHQ49/T5/840). Cultures were constantly mixed using magnetic PTFE stirrer bars and aerated with a filtered (0.2 μm pore) air mixture at a rate of ~200 ml s^{-1}. The CO_2 concentration was regulated (±2 μmol mol^{-1}) by mass-flow controllers (Bronkhorst, Newmarket, UK) and CO_2-free air was supplied by an oil-free compressor (Bambi Air, UK) via a soda-lime gas-tight column that was mixed with a 10% CO_2-in-air mixture from a gas cylinder (BOC Industrial Gases, UK). The CO_2 concentration in the gas phase was continuously monitored by an infra-red gas analyser (Li-Cor Li-820, Lincoln, NE, USA), calibrated weekly against a standard gas (BOC Industrial Gases).

Cultures were kept at the upper section of the exponential growth phase through periodic dilution with new growth media at 3–5 d intervals. Daily growth rates were quantified from changes in baseline fluorescence (F_o) measured between 09.00 h and 10.30 h on dark-adapted cultures (20 min) using a FRRfII FastAct Fluorometer System (Chelsea Technologies Group Ltd, UK). As detailed in Boatman *et al.* (2018*a*), cultures were deemed fully acclimated and in balanced growth when both the slope of the linear regression of ln(F_o) and the ratio of live-cell to acetone-extracted F_o were constant following every dilution with fresh YBCII medium.

The Ci chemistry was measured prior to the dilution of each culture with fresh media, where exactly 20 ml of culture from each treatment was filtered through a swinnex filter (25 mm, 0.45 μm pore, glass fibre filter): 15 ml into a plastic centrifuge tube (no headspace) for TIC analysis (Shimadzu TOC-V Analyser & ASI-V Autosampler), and 5 ml into a plastic cryogenic vial (Sigma-Aldrich V5257-250EA; no headspace) for pH analysis. The bicarbonate (HCO_3^-), carbonate (CO_3^{2-}), and CO_2 concentrations were calculated via *CO2SYS* as described in Boatman *et al.* (2017). Overall, the CO_2 drawdown in the cultures ranged between 49 μmol mol^{-1} and 90 μmol mol^{-1} for all CO_2 treatments (Table 1) and exhibited a negligible CO_2 drift over a diurnal cycle (see Supplementary Fig. S1 at *JXB* online).

Gross and net O_2 exchange

Light-dependent rates of O_2 production and consumption were measured on four biological replicates per CO_2 treatment, using a membrane inlet mass spectrometer (MIMS) and an $^{18}O_2$ technique modified from McKew *et al.* (2013).

Table 1. *The growth conditions (±SE) achieved for* T. erythraeum *IMS101 when cultured at three target gas phase $ChlCO_2$ concentrations (low=180 µmol mol^{-1}, mid=380 µmol mol^{-1}, and high=720 µmol mol^{-1}), saturating light intensity (400 µmol photons m^{-2} s^{-1}), and optimal temperature (26 °C)*

Variables	Units	Low-CO_2	Mid-CO_2	High-CO_2
pH	–	8.461	8.175	7.905
H^+	nM	3.5 (0.1)	6.7 (0.1)	12.5 (0.2)
A_T	µM	2427 (32)	2490 (51)	2444 (42)
TCO_2	µM	1797 (30)	2076 (44)	2204 (37)
HCO_3^-	µM	1356 (30)	1773 (37)	2008 (32)
CO_3^{2-}	µM	436 (9)	295 (8)	179 (5)
CO_2	µM	3.3 (0.2)	8.2 (0.2)	17.4 (0.3)
NH_4^+	mM	1.00 (0.12)	1.06 (0.08)	1.02 (0.06)
NO_3^-	mM	0.33 (0.05)	0.36 (0.02)	0.32 (0.02)
n		76	32	28

Individual pH values were converted to a H^+ concentration, allowing a mean pH value to be calculated. Dissolved inorganic NH_4^+ was determined using the phenol-hypochlorite method as described by Solorzano (1969), while dissolved inorganic NO_3^- was determined using the spectrophotometric method as described by Collos *et al.* (1999).

MIMS samples were prepared by placing 300 ml of culture in a large gas-tight syringe, and gently bubbled with N_2 gas for ~20 min to reduce the $^{16}O_2$ concentration. The headspace was removed, and 2 ml of $^{18}O_2$ gas (CK Gas Products, UK; 99% purity) was added and mixed by continuously inverting the syringe for 20 min. During this process, the culture was maintained at a low light intensity (<10 µmol photons m^{-2} s^{-1}) and at growth temperature (26 °C). Samples were incubated using a series of 6 ml glass stopper, gas-tight test tubes, which were cleaned with detergent, acid-washed (10% HCl for 1 d), and rinsed with deionized water (Millipore Milli-Q Biocel, ZMQS60FOI) prior to use. Glass beads were placed inside each test tube, allowing the sample to be mixed throughout the incubation. The $^{18}O_2$-enriched culture was quickly dispensed into the gas-tight glass test tubes, sealed using ground glass stoppers (no headspace), and immediately placed into a temperature-controlled (26 °C) incubator. A white light-emitting diode (LED) block (Iso Light 400, Technologica, Essex, UK) was positioned at one end of the incubator, generating light intensities ranging from 10 µmol photons m^{-2} s^{-1} to 1100 µmol photons m^{-2} s^{-1}.

For each replicate, 24 test tubes were incubated across the light gradient, a minimum of 10 test tubes were used to determine the initial concentration of O_2 isotopes, and an additional four test tubes were incubated in the dark (26 °C) to determine dark respiration rates. All photosynthesis–light (P–E) response curves were measured at the same time of day between 4 h and 6 h into the photo-phase of the L/D cycle and were incubated for between 60 min and 120 min. Culture densities for these experiments ranged from 80 µg Chl *a* l^{-1} to 240 µg Chl *a* l^{-1}.

Changes in $^{16}O_2$ and $^{18}O_2$ and thus O_2 consumption (U_0) and O_2 evolution (E_0) were calculated using the following equations (Radmer and Kok, 1976);

$$U_0 = -\left(1+\frac{^{16}O_2}{^{18}O_2}\right)\cdot\frac{\Delta^{18}O_2}{\Delta t} \quad (1)$$

$$E_0 = \frac{\Delta^{16}O_2}{\Delta t} - \left(\frac{^{16}O_2}{^{18}O_2}\right)\cdot\frac{\Delta^{18}O_2}{\Delta t} \quad (2)$$

where U_0 is the rate of O_2 consumption and E_0 is the rate of gross O_2 evolution. C-specific rates were obtained by dividing U_0 and E_0 by the concentration of particulate organic carbon (POC). Rates were also normalized to Chl *a* and particulate organic nitrogen (PON), and are presented in Supplementary Figs S2 and S3.

The P–E curves for gross (E_{0C}) and net O_2 exchange (P_{nC}=E_{0C}–U_{0C}) were fitted to the following equations from Platt and Jassby (1976);

$$E_{0C} = E_{0C,max}\bullet\left[1-e\left(\frac{-\alpha_{gC}\cdot E}{E_{0C,max}}\right)\right] \quad (3)$$

$$P_{nC} = P_{nC,max}\bullet\left[1-e\left(\frac{-\alpha_{nC}\cdot E}{P_{nC,max}}\right)\right] + R_{dC} \quad (4)$$

where $E_{0C,max}$ and $P_{nC,max}$ are the carbon-specific maximum gross and net O_2 evolution rates; α_{gC} and α_{nC} are the carbon-specific initial light-limited slopes for gross and net photosynthesis; R_{dC} is the dark respiration rate; and E is the light intensity (µmol photons m^{-2} s^{-1}). Curve fitting was performed on each biological replicate separately to calculate mean (±SE) curve fit parameterizations (Sigmaplot 11.0).

The maximum quantum efficiencies of gross ($\phi_{m,g}$) and net ($\phi_{m,n}$) O_2 evolution were calculated as follows;

$$\phi_{m,g} = \frac{\alpha_{gC}}{a_{C,eff}} \quad (5)$$

$$\phi_{m,n} = \frac{\alpha_{nC}}{a_{C,eff}} \quad (6)$$

where the C-specific initial slope for gross (α_{gC}) or net (α_{nC}) O_2 evolution, spectrally corrected to the culturing LEDs (Supplementary Fig. S6), was divided by the C-specific, spectrally corrected effective light absorption coefficient ($a_{C,eff}$).

Spectrophotometric Chl a *and POC analysis*

Samples for the determination of Chl *a* and POC were collected with each light–response curve, while PON was calculated from the measured POC using the CO_2-specific C:N ratio reported in Boatman *et al.* (2018*a*). For measurements of Chl *a* and POC, two 100 ml samples from each culture were vacuum-filtered onto pre-combusted 25 mm glass fibre filters (0.45 µm pore; Fisherbrand FB59451, UK). The first filter was dried at 60 °C and the POC quantified using a TC analyser (Shimadzu TOC-V Analyser & SSM-5000A Solid Sample Combustion Unit). The second filter was placed in 5 ml of 100% methanol, homogenized, and extracted overnight at –20 °C, before being centrifuged at 12 000 *g* for 10 min, and a 3 ml aliquot of the supernatant added to a quartz cuvette. The absorption spectrum (400–800 nm) was measured using a (Hitachi U-3000, Japan) spectrophotometer and the Chl *a* concentration (µg l^{-1}) was calculated using the following equation (Ritchie, 2008);

$$\text{Chl}\,a = \left[\frac{\left(12.9447\cdot\left(Abs_{665}-Abs_{750}\right)\right)\cdot Vol_E}{Vol_F}\right]\cdot 1000 \quad (7)$$

where Abs_{665} and Abs_{750} are the baseline-corrected optical densities of the methanol-extracted sample at 665 nm and 750 nm; Vol_E is the volume of the solvent used for extraction (i.e. 5 ml); Vol_F is the volume of culture filtered (i.e. 100 ml), and 12.9447 is a cyanobacteria-specific Chl *a* coefficient for 100% methanol extraction.

Supporting spectrophotometric measurements were made on live cells using an integrating sphere to determine the *in vivo* light absorption (Supplementary File SI). From this we determined biomass-specific (Chl *a*, C, and N) light absorption coefficients under the varying CO_2 treatments (Supplementary Fig. S4), reconstructed the light absorption spectra from photosynthetic pigment spectra (Supplementary File SII; Supplementary Table S1), and calculated maximum quantum efficiencies of gross and net O_2 evolution (Table 3).

Results

Growth rate, cell composition, and light absorption

Balanced growth rates increased from 0.2 d^{-1} at low-CO_2 to 0.34 d^{-1} at mid-CO_2 and 0.36 d^{-1} at high-CO_2 (Table 2). Chl *a*:C ratios were lowest under low-CO_2 conditions and were significantly higher in the mid-CO_2 treatment relative to the low- and high-CO_2 treatments (Table 2).

Light dependence of O_2 exchange

The C-specific maximum rate ($E_{0C,max}$) and initial slope (α_{gC}) of light-dependent gross photosynthesis were significantly higher in the mid-CO_2 treatment relative to the low- and high-CO_2 treatments (Table 3). Conversely, the light saturation parameter ($E_k=E_{0C,max}/\alpha_{gC}$) for gross O_2 evolution (Table 3) and the maximum quantum efficiency of gross O_2 evolution ($\phi_{m,g}=\alpha_{gC}/a_{C,eff}$) (Table 3) did not vary significantly amongst the CO_2 treatments due to co-variation of α_{gC} and $E_{0C,max}$.

Table 2. *The mean (±SE) balanced growth rate and Chl a:C ratio for* T. erythraeum *IMS101 when acclimated to three target CO_2 concentrations (low=180 µmol mol^{-1}, mid=380 µmol mol^{-1}, and high=720 µmol mol^{-1}), saturating light intensity (400 µmol photons m^{-2} s^{-1}), and optimal temperature (26 °C)*

Variables	Units	Low-CO_2	Mid-CO_2	High-CO_2
Growth rate	d^{-1}	0.198 (0.027) A	0.336 (0.026) B	0.361 (0.020) B
Chl *a*:C	g:mol	0.052 (0.003) A	0.089 (0.003) C	0.066 (0.003) B

Abbreviations: Chl *a*:C ratios are g:mol (n=9 at low-CO_2, n=6 at mid- and high-CO_2). Letters indicate significant differences between CO_2 treatments (one-way ANOVA, Tukey post-hoc test; P<0.05); where B is significantly greater than A, and C is significantly greater than B and A.

The C:N ratios reported by Boatman *et al.* (2018*a*) for the low-, mid-, and high-CO_2 treatments (7.9, 7.8, and 7.3 mol:mol, respectively) were not significantly different. As such, the CO_2 response of N-specific maximum rates and light-limited initial slopes of gross O_2 evolution were comparable with C-specific rates (Supplementary Fig. S2; Supplementary Table S2). The ~2-fold variability of $E_{0C,max}$ and α_{gC} was largely due to differences in the Chl *a*:C ratio, with the Chl *a*-specific light absorption varying by only 1% across CO_2 treatments (Supplementary Table S1).

The C-specific dark respiration rates (R_{dC}) varied by ~10% amongst CO_2 treatments (Table 3). The maximum net O_2 evolution rate ($P_{nC,max}$) approximately doubled from the low-CO_2 to the mid- and high-CO_2 treatments, but did not differ between mid- and high-CO_2, with the initial slope (α_{nC}) showing a similar pattern to $P_{nC,max}$ (Table 3). Similar responses were observed for the maximum rate ($V_{C,max}$) and initial slope (Affinity) of the CO_2 dependency of C fixation as reported in Boatman *et al.* (2018*a*).

The relationship between P_n and E_0 was linear (Fig. 1), with the slope increasing by ~13% from low- to mid-CO_2 and by 22% from mid- to high-CO_2 (Table 4). This linear relationship indicates that light-dependent O_2 consumption (U_{0C}) was a constant proportion of gross O_2 evolution (E_{0C}), independent of light intensity under each of the CO_2 treatments. Subtracting the slope from unity gives the ratio of light-dependent O_2 consumption to gross O_2 evolution, which declined significantly from 0.79 at high-CO_2 to 0.65 at mid-CO_2 and 0.57 at low-CO_2.

Photosynthetic quotient

We calculated the photosynthetic quotient (PQ) as:

$$PQ = \frac{(P_{nC})}{V_C} \quad (8)$$

Table 3. *The physiological parameters (±SE) of the C-specific light–response curves for the gross and net photosynthetic O_2 evolution of* T. erythraeum *IMS101 (n=4) measured using the MIMS light source*

Parameters	Units	Low-CO_2	Mid-CO_2	High-CO_2
Gross O_2 evolution				
$E_{0C,max}$	mmol O_2 (g C)$^{-1}$ h^{-1}	1.875 (0.118) A	3.795 (0.175) C	2.973 (0.158) B
E_k	µmol photons m^{-2} s^{-1}	277 (15)	250 (20)	281 (15)
α_{gC}	µmol O_2 (g C)$^{-1}$ h^{-1} (µmol photons m^{-2} s^{-1})$^{-1}$	6.78 (0.33) A	15.35 (0.82) C	10.58 (0.18) B
$\phi_{m,g}$	mol O_2 (mol photons)$^{-1}$	0.037 (0.004)	0.042 (0.004)	0.045 (0.003)
Net photosynthesis				
$P_{nC,max}$	mmol O_2 (g C)$^{-1}$ h^{-1}	1.131 (0.061) A	2.534 (0.287) B	2.312 (0.140) B
E_k	µmol photons m^{-2} s^{-1}	300 (41)	270 (24)	270 (10)
α_{nC}	µmol O_2 (g C)$^{-1}$ h^{-1} (µmol photons m^{-2} s^{-1})$^{-1}$	3.94 (0.46) A	9.48 (1.02) B	8.57 (0.35) B
R_{dC}	mmol O_2 (g C)$^{-1}$ h^{-1}	–0.600 (0.078)	–0.644 (0.132)	–0.659 (0.013)
$\phi_{m,n}$	mol O_2 (mol photons)$^{-1}$	0.020 (0.002) A	0.026 (0.003) A	0.037 (0.002) B
Slopes				
P_{nC} versus E_{0C}	Dimensionless	0.571 (0.028) A	0.646 (0.046) A	0.791 (0.017) B
U_{0C} versus E_{0C}	Dimensionless	0.429 (0.028) B	0.354 (0.046) A	0.209 (0.017) A
U_{0C} versus P_{nC}	Dimensionless	0.701 (0.073) B	0.553 (0.111) B	0.254 (0.024) A

Abbreviations: $E_{0C,max}$, the C-specific maximum gross O_2 evolution rate; $P_{nC,max}$, the C-specific maximum net O_2 evolution rate; E_k, the light saturation parameter; α_{gC} and α_{nC} are the C-specific initial slopes of the light–response curve for net and gross photosynthesis; $\phi_{m,g}$ and $\phi_{m,n}$ are the maximum quantum efficiencies of gross and net O_2 evolution calculated using the absorption coefficients reported in Supplementary Table S1; R_{dC}, the C-specific dark respiration rate; Slope=the slope of the regression of E_{0C} against P_{nC}, E_{0C} against O_2 uptake (U_{0C}), and U_{0C} against P_{nC}. Letters indicate significant differences between CO_2 treatments (one-way ANOVA, Tukey post-hoc test; P<0.05); where B is significantly greater than[A, and C is significantly greater than B and A.

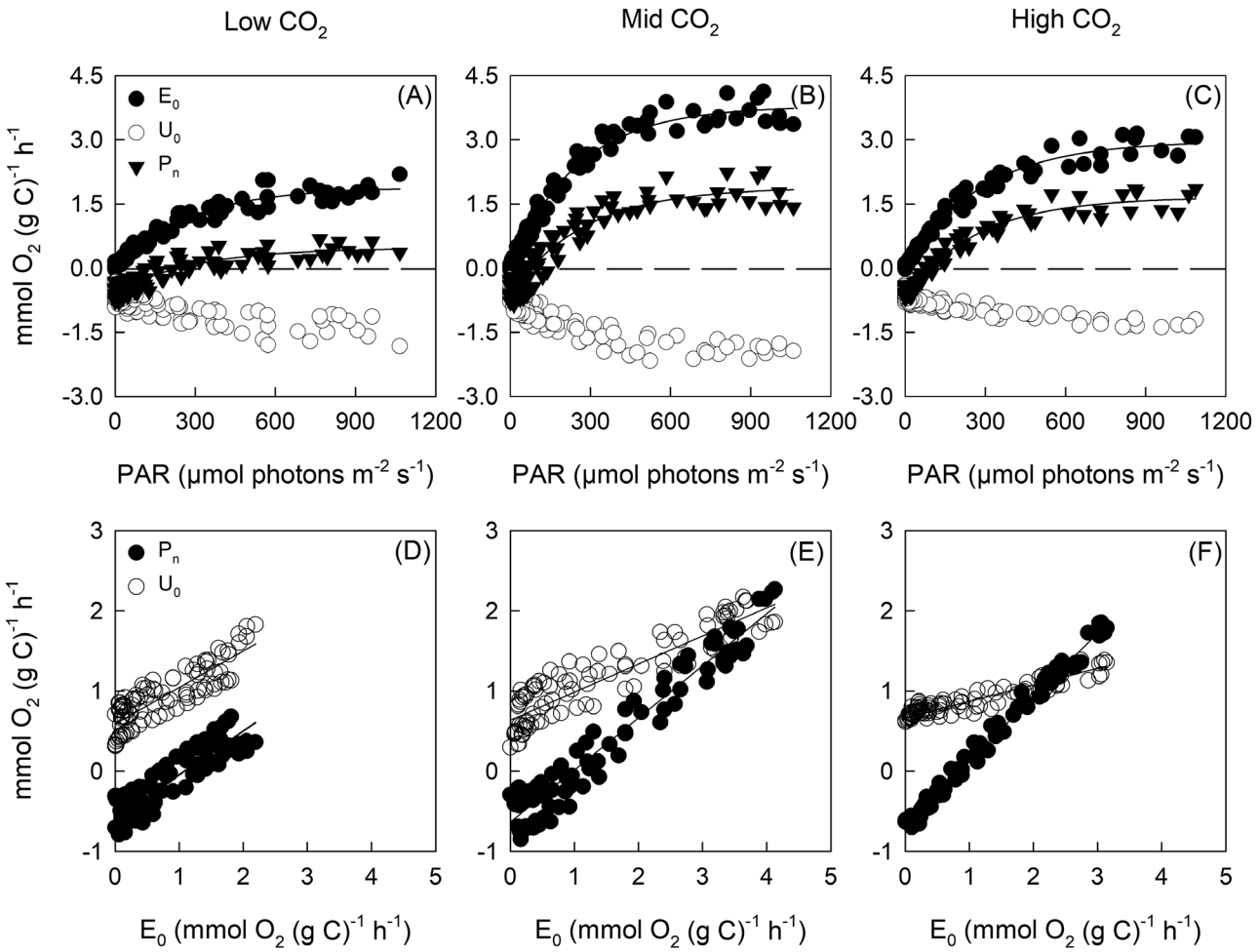

Fig. 1. The C-specific light–response curves for gross O_2 evolution, O_2 consumption, and net photosynthesis (n=4) (A–C) and the relationship between gross net O_2 evolution and net O_2 evolution or O_2 consumption (D–F) for *T. erythraeum* IMS101. Oxygen evolution rates are normalized to a carbon basis [mmol O_2 (g C)$^{-1}$ h^{-1}]. The dashed line represents where gross O_2 evolution equals O_2 consumption (i.e. net photosynthesis=0). Note, Chl *a*- and N-specific light–response curves are reported in Supplementary Figs S2 and S3.

where P_{nC} is the C-specific net O_2 evolution rate (E_0–U_0) and V_C is the C-specific C-fixation rate reported by Boatman *et al.* (2018*a*), with both P_{nC} and V_C calculated at the growth light intensity (400 mmol photon m^{-2} s^{-1}) and growth CO_2 concentration (Table 1). The *PQ* calculated in this way (Table 4) did not vary systematically amongst the CO_2 treatments, averaging about 1.15 mol O_2 mol CO_2^{-1}.

A second value of *PQ* was calculated by dividing E_{0C} by V_C for C fixation under the corresponding conditions, which increased from 1.3 mol O_2 mol CO_2^{-1} in the high-CO_2 treatment to ~2.0 mol O_2 mol CO_2^{-1} for the low- and mid-CO_2 treatments (Table 4), reflecting the increase in light-dependent O_2 consumption with decreasing CO_2.

Discussion

Effect of acclimation to variation of inorganic chemistry on growth rates and the Chl a:carbon ratio

The increased growth rate from low- (180 µmol mol^{-1}) to mid- (380 µmol mol^{-1}) and high-CO_2 (720 µmol mol^{-1}) was similar to previous findings (Barcelos e Ramos *et al.*, 2007; Boatman *et al.*, 2017, 2018*b*). Whilst not statistically significant, balanced growth rates were ~10% greater at high-CO_2 than at mid-CO_2. The magnitude of this increase is comparable with several recent studies, which show rates increasing by 7–26% at similar CO_2 concentrations (Barcelos e Ramos *et al.*, 2007; Hutchins *et al.*, 2007; Levitan *et al.*, 2007; Kranz *et al.*, 2010; Garcia *et al.*, 2011; Boatman *et al.*, 2017).

We observed that the Chl *a*:C ratio varied 1.7-fold, peaking in the mid-CO_2 treatment (Table 2). This is in contrast to previous research which showed that both Chl *a*:C and growth rate were largely independent of CO_2 in *Trichodesmium* (Kranz *et al.*, 2009, 2010). One possible explanation for the difference between our study and previous research is that we grew *Trichodesmium* at a higher light intensity (400 µmol photons m^{-2} s^{-1} in our experiments; 200 µmol photons m^{-2} s^{-1} used by Kranz *et al.*), and that pigment synthesis was down-regulated in our low-CO_2 treatment where CO_2 limited growth rate. Down-regulation of pigment synthesis by CO_2 limitation on growth was also observed previously for *Synechococcus* by Fu *et al.* (2007). In contrast, we hypothesize that the reduction in Chl *a*:C that we observed from mid-CO_2 to high-CO_2 may be due to the reduced cost of operating a CCM at high-CO_2.

Table 4. *The photosynthetic quotients (±SE) for* T. erythraeum *IMS101, calculated from the light-saturated, maximal rates of carbon-specific O_2 evolution, and the C fixation rates*

Parameters	Units	Low-CO_2	Mid-CO_2	High-CO_2
Photosynthetic quotient				
E_{0C}/V_C	mol O_2 (mol C)$^{-1}$	1.98 (0.10)	1.99 (0.04)	1.28 (0.04)
P_{nC}/V_C	mol O_2 (mol C)$^{-1}$	1.14 (0.07)	1.29 (0.11)	1.01 (0.05)

V_C was calculated as $V_C=(V_{C,max}\times[CO_2])/(K_m+[CO_2])$ using the value of K_m from Boatman *et al.* (2018*a*) and $[CO_2]$ from Table 1. E_{0C} was calculated as $E_{0C}=E_{0C,max}\times[1-e(-\alpha\times E/E_{0C,max})]$ and P_{nC} was calculated as $P_{nC}=P_{nC,max}\times[1-e(-\alpha\times E/P_{nC,max})]$ using E=400 µmol photons m^{-2} s^{-1} and values of E_k from Table 3.

Dark respiration and maintenance metabolic rate

Maintenance metabolism is a collection of key functions necessary to preserve cell viability that are commonly assumed to be independent of growth rate and as such can be estimated by extrapolating the relationship between light-limited growth rate and light intensity (E) to E=0 (Geider and Osborne, 1989). We estimated a maintenance metabolic rate [0.034 d^{-1} ~0.12 mmol O_2 (g C)$^{-1}$ h^{-1}] from previous observations of the light dependence of *Trichodesmium* growth (Boatman *et al.*, 2017; Supplementary Fig. S5). In the dark, *Trichodesmium* has a respiration rate [R_d=0.60–0.66 mmol O_2 (g cellular C)$^{-1}$ h^{-1}] (Table 3) that is about five times higher than what is needed to maintain cellular metabolism. In most cyanobacteria, dark respiration rates (R_d) are a small proportion of light-saturated net O_2 production rates ($P_{n,max}$) (Matthijs and Lubberding, 1988; Geider and Osborne, 1989). In contrast, we observed R_d rates that were a high proportion of light-saturated photosynthesis, consistent with other reports of high ratios of R_d to net photosynthesis in natural (Kana, 1993) and cultured *Trichodesmium* (Berman-Frank *et al.*, 2001; Kranz *et al.*, 2010; Eichner *et al.*, 2017). For *Trichodesmium* spp., a high R_d is required to support the rates of N_2 fixation measured in darkness. N_2 fixation is energetically expensive, requiring a minimum consumption of 13 ATP and 6 reducing equivalents per N_2 fixed, assuming complete recycling of H_2 produced by nitrogenase to recover ATP.

From our observed growth rates and the C:N ratio reported by Boatman *et al.* (2018*a*), we calculate that the O_2 consumption rate required to support the level of N_2 fixation needed for growth is ~0.5 mmol O_2 (g C)$^{-1}$ h^{-1} in cells grown under low-CO_2, increasing to ~1 mmol O_2 (g C)$^{-1}$ h^{-1} in cells grown under high-CO_2 (Supplementary File SIII). These rates are of the same order as R_d [0.60–0.66 mmol O_2 (g C)$^{-1}$ h^{-1}] (Table 3), indicating that R_d may provide a substantial proportion of the ATP and reductant required for N_2 fixation in the light. Significantly, Kana (1993) found that the addition of DCMU to illuminated cells caused the rate of oxygen uptake (U_0) to decline to the rate observed in darkness, opening up the possibility that continuation of the 'dark' respiration rate in the light provides at least some of the energy required for N_2 fixation.

Effect of acclimation to pCO_2 on gross photosynthesis and photosynthetic quotients

Carbon-specific rates are directly related to changes in the specific growth rate, as both rates can be expressed in equivalent units of inverse time (e.g. h^{-1} or d^{-1}). However, due to differences in the Chl *a*:C ratio (Table 2), Chl *a*-specific maximum rates ($E_{0Chl,max}$) and initial slopes (α_{gChl}) of light-dependent gross photosynthesis did not differ significantly between CO_2 treatments (Supplementary Fig. S3; Supplementary Table S3), an observation that is consistent with the findings reported by Levitan *et al.* (2007) and Eichner *et al.* (2014). We suggest that the reduced Chl *a*:C ratio at low-CO_2 relative to mid-CO_2 is probably due to the cost of up-regulating the CCM, whereas the reduced Chl *a*:C ratio at high-CO_2 relative to mid-CO_2 may be due to an increase in carbohydrate storage granules.

In contrast to $E_{0C,max}$, which clearly peaked in the mid-CO_2 treatment, the maximum net O_2 evolution rate ($P_{nC,max}$) increased from low- to mid-CO_2 but was not statistically different between mid- and high-CO_2 treatments (Table 3). The 2-fold increase of $P_{nC,max}$ from low- to mid- and high-CO_2 is consistent with the effect of CO_2 on growth rate.

Dividing the rate of net O_2 evolution (P_{nC}) by the rate of C fixation under comparable light and CO_2 conditions gave values for the *PQ* that ranged from 1.0 mol O_2 to 1.3 mol O_2 evolved per mol CO_2 fixed (Table 4). A *PQ* of 1.0 is expected if carbohydrate is the major product of photosynthesis as P_{nC} measures the light-driven electron transport from PSII to NADPH, which then feeds into CO_2 assimilation by the Calvin cycle. A *PQ* >1.0 is expected if recent photosynthate is used in synthesis of compounds that are more reduced than carbohydrates (e.g. lipid) and/or that photosynthetically generated reductant is used to power N_2 fixation and N assimilation into amino acids. Alternatively or in addition, a slightly higher *PQ* may be required if photosynthetically generated reductant is required for operation of the CCM, or for salvaging CO_2 that leaks from carboxysomes by conversion of CO_2 to HCO_3^- by NDH-I_4 (Price *et al.* (2008). This corroborates our findings, where under high-CO_2, when the CCM is probably down-regulated, we observed a *PQ* value close to 1.0. Conversely at low- and mid-CO_2, when more energy is required for the CCM, we observed a *PQ* value >1.0.

Effect of acclimation to pCO_2 on light-stimulated O_2 consumption and the relationship between net and gross O_2 evolution

We found that O_2 consumption rates (U_0) of *Trichodesmium* increased markedly with light intensity, with U_0 saturating at a similar light intensity to gross O_2 evolution (Fig. 1). This suggests that light-driven U_0 increased in parallel with gross O_2 evolution and that dark respiration continued at similar rates in the light and dark. Previously, Kana (1993) observed a very slight decline in U_0 between darkness and low-light intensity in natural *Trichodesmium* colonies, followed by parallel increases of U_0 and O_2 evolution (E_0) with increasing light. Kana (1993) attributed the light-stimulated component of U_0 to the Mehler reaction, as the addition of DCMU to illuminated cells caused U_0 to decline to the rate observed in darkness.

The slope of the dependence of U_{0C} on E_{0C} decreased with increasing growth CO_2 from 0.43 in cultures grown under low-CO_2 to 0.21 in cultures grown under high-CO_2 (Table 3). Thus, the light-driven component of U_0 decreased from ~43% of E_0 in the low-CO_2 culture to 21% of E_0 in the high-CO_2

culture. Pseudocyclic photophosphorylation coupled to the consumption of O_2 associated with the Mehler reaction can provide ATP that may be used to support N_2 fixation, CO_2 fixation, or for operating a CCM (Miller *et al.*, 1988). The linearity between U_0 and E_0 suggests that light-dependent O_2 consumption may be required to balance the ratio of ATP production to NADPH production in the light reactions of photosynthesis. As the photon efficiency of ATP production by pseudocyclic photophosphorylation is the same as that of photophosphorylation driven by linear photosynthetic electron transport (LPET) (Baker *et al.*, 2007), our results suggest that 26% more ATP than can be generated by LPET is required by cells growing under high-CO_2, increasing to 55% more ATP in cells growing under mid-CO_2 and 75% more ATP in cells growing under low-CO_2. Much of the additional ATP that could be generated by pseudocyclic photophosphorylation may be accounted for by the ATP requirements for CO_2 fixation by the Calvin cycle (1.5 ATP/e^-) and N_2 fixation (2.1 ATP/e^-) being greater than the ratio of ATP to reducing equivalents generated by LPET (1.25 ATP/e^-). At low-CO_2, the increase in U_0 may also be required to operate a CCM, as observed in the freshwater *Synechococcus* (Miller *et al.*, 1988).

An estimate of the cost of operating the CCM

Stimulation of growth and productivity of *T. erythraeum* IMS101 in response to increasing CO_2 is commonly attributed to reductions in the amount of energy required for establishing, maintaining, and operating a CCM (Hutchins *et al.*, 2007, 2015; Levitan *et al.*, 2007; Garcia *et al.*, 2011). Two aspects for the cost of operating the CCM in *Trichodesmium* are those for HCO_3^- transport into the cell, which must balance CO_2 fixation and CO_2 leakage, and those for retaining inorganic C within the cell by converting CO_2 that diffuses from the carboxysome to HCO_3^- via the NDH-I_4 CO_2 uptake/salvage system. The cost of HCO_3^- transport of ~1 ATP for each C transported into the cell (Raven *et al.*, 2014) could be supplied by either cyclic photosynthetic electron transfer around PSI or pseudocyclic photosynthetic electron transfer linked to the Mehler reaction. As the ratio of CO_2 leakage to gross inorganic C uptake has been found to be independent of pCO_2 over the range of 150–1000 μmol mol^{-1} (Kranz *et al.*, 2009, 2010), the ATP required for HCO_3^- transport will also be independent of pCO_2.

Rather than fuelling ATP production by pseudocyclic electron transport, light-dependent O_2 consumption may be a consequence of operating the NDH-I_4 CO_2 uptake/salvage system. For *Trichodesmium*, the NDH-I_4 protein is thought to reduce the efflux of CO_2 from the cell, converting it to HCO_3^- but at a cost of consuming reducing equivalents [NADPH or reduced ferredoxin (F_d)] (Price *et al.*, 2008).

The stoichiometry based on NADPH as the electron donor can be represented as:

$$2\ \mathrm{NADPH} + 2\ \mathrm{CO_2} + \mathrm{O_2} \rightarrow 2\ \mathrm{HCO_3^-} + 2\ \mathrm{NADP^+} \quad (9)$$

If NDH-I_4 activity is employed to minimize CO_2 effluxes, then the rate of O_2 consumption associated with this process would be expected to decrease with increases of extracellular CO_2 concentration. As NADPH consumption by this mechanism is closely linked in time and space to NADPH production via LPET, this process would be inhibited by DCMU in a similar manner to the Mehler reaction.

Roles of photosynthetic and respiratory metabolism in N_2 fixation

Increased pCO_2 will not only stimulate CO_2 fixation, but will also stimulate N_2 fixation (dependent on carbon skeletons for sequestration of the ammonium produced) and growth in *Trichodesmium* (Barcelos e Ramos *et al.*, 2007; Hutchins *et al.*, 2007; Levitan *et al.*, 2007, 2010*b*; Kranz *et al.*, 2009, 2010). This is probably in response to energy relocation from the CCM (Badger *et al.*, 2006; Kranz *et al.*, 2011) toward CO_2 and N_2 fixation (Levitan *et al.*, 2007; Kranz *et al.*, 2011).

Diazocytes may use the light reactions of photosynthesis to provide some or most of the ATP required to support N_2 fixation either through cyclic photophosphorylation associated with electron transfer around PSI or through pseudocyclic photophorylation involing LPET from H_2O to O_2 involing both PSII and PSI. However, LPET evolves O_2, which is known to inactivate nitrogenase. Enhanced rates of the Mehler reaction, unless uncoupled from O_2 evolution at PSII, will not affect the O_2 balance of diazocytes. However, if respiration provides the ATP for N_2 fixation, then sugars and/or organic acids may be produced by photosynthesis in diazocytes prior to the initiation of N_2 fixation (temporal separation of CO_2 fixation from N_2 fixation) or in other cells within the trichome and transported laterally into the diazocytes (spatial separation of CO_2 fixation from N_2 fixation).

Temporal separation of N_2 fixation from photosynthetic O_2 evolution may be achieved if glycogen that accumulates in diazocytes prior to the onset of N_2 fixation provides the reducing equivalents and ATP to fuel N_2 fixation, perhaps supplemented by high rates of cyclic photosynthetic electron transfer around PSI to generate ATP. Temporal separation is consistent with the pattern of CO_2 fixation and N_2 fixation observed in *Trichodesmium* where the former peaks earlier in the day than the latter (Berman-Frank *et al.*, 2001). Spatial separation has been observed in heterocystous cyanobacteria where transport of sugars into heterocysts from surrounding cells can be respired to fuel N_2 fixation (Wolk, 1968; Böhme, 1998). Although we are not aware of direct evidence for rapid transfer of metabolites amongst cells along a trichome, such a transfer would be consistent with observations of Finzi-Hart *et al.* (2009), showing that all cells within a *Trichodesmium* trichome show the same temporal pattern of accumulation and mobilization of cyanophycin granules and the same temporal pattern of labelling with $^{13}CO_2$ and ^{15}N.

Conclusion

In this study, we accredit the bell-shaped CO_2 response of the C-specific maximum gross photosynthesis rates ($E_{0C,max}$) to the CCM, where the 2-fold increase in $E_{0C,max}$ from low- to mid-CO_2 supports the almost 2-fold increase in balanced growth rates

and the decrease in $E_{0C,max}$ from mid- to high-CO_2 is due to less expenditure on the CCM whilst cells grow at a similar rate.

Our results indicate a significant decrease in the ratio of the rate of light-driven O_2 consumption to the rate of gross photosynthetic O_2 evolution with increasing CO_2, which probably arises from a reduced cost of operating the CCM. In addition, dark respiration appears to be sufficient to provide much of the energy required to support significant rates of N_2 fixation, even in the light.

We have not extrapolated our findings to a full day as light–response curves were measured at one time point and *Trichodesmium* exhibits pronounced diurnal variability in photosynthetsis and N_2 fixation (Berman-Frank *et al.*, 2001). In addition, extrapolating to future conditions in the natural environment should consider (i) the impact of adaptation of *Trichodesmium* to future conditions (Hutchins *et al.*, 2015); (ii) strain and clade variability (Hutchins *et al.*, 2013); and (iii) additional integrated effects of abiotic variables other than CO_2 (i.e. light intensity, temperature, and nutrients such as P and Fe) (Walworth *et al.*, 2016).

In the context of open oceans, nutrient-replete P_n and growth rates of *T. erythraeum* IMS101 would have been severely CO_2 limited at the last glacial maximum relative to current conditions. Future increases of CO_2 may not significantly increase growth and productivity of *Trichodesmium*, although increases in key stoichiometric ratios (N:P and C:P) as reported by Boatman *et al.* (2018*a*) may affect bacterial and zooplankton metabolism, the pool of bioavailable N, the depth at which sinking organic matter is remineralized, and consequently carbon sequestration via the biological carbon pump (Mulholland *et al.*, 2004; McGillicuddy, 2014). These responses could serve as a negative feedback to climate change by increasing new N and C production, thereby increasing the organic carbon sinking to the deep ocean.

Supplementary data

Supplementary data are available at *JXB* online.

Table S1. The measured and modelled effective light absorption coefficients and relative photosynthetic pigment contribution to the total light absorption.

Table S2. The physiological parameters of the N-specific light–response curves for gross and net photosynthetic O_2 evolution of *T. erythraeum* IMS101.

Table S3. The physiological parameters of the Chl *a*-specific light–response curves for gross and net photosynthetic O_2 evolution of *T. erythraeum* IMS101.

Table S4. Values of the goodness of fit for the C-specific light–response curves for gross and net photosynthetic O_2 evolution of *T. erythraeum* IMS101.

Table S5. The Chl *a*-specific photosynthetic quotients of *T. erythraeum* IMS101.

Fig. S1. The inorganic carbon chemistry of *T. erythraeum* IMS101 cultures over the light period.

Fig. S2. The N-specific light–response curves for gross O_2 evolution, O_2 consumption, and net photosynthesis for *T. erythraeum* IMS101.

Fig. S3. The Chl *a*-specific light–response curves for gross O_2 evolution, O_2 consumption, and net photosynthesis for *T. erythraeum* IMS101.

Fig. S4. The measured and modelled *in vivo* light absorption spectra for *T. erythraeum* IMS101.

Fig. S5. The light compensation point of *T. erythraeum* IMS101 growth.

Fig. S6. The relative emission spectra of the culturing and MIMS LEDs and the spectral corrected light absorption spectra of *T. erythraeum* IMS101.

File S1. *In vivo* light absorption.

File S2. Modelling the *in vivo* light absorption from pigment absorption spectra.

File S3. Stoichiometry and energetics of N_2 fixation.

Acknowledgements

TGB was supported by a UK Natural Environment Research Council PhD studentship (NE/J500379/1 DTB).

References

Badger MR, Palmqvist K, Yu JW. 1994. Measurement of CO_2 and HCO_3^- fluxes in cyanobacteria and microalgae during steady-state photosynthesis. Physiologia Plantarum **90,** 529–536.

Badger MR, Price GD, Long BM, Woodger FJ. 2006. The environmental plasticity and ecological genomics of the cyanobacterial CO_2 concentrating mechanism. Journal of Experimental Botany **57,** 249–265.

Baker NR, Harbinson J, Kramer DM. 2007. Determining the limitations and regulation of photosynthetic energy transduction in leaves. Plant, Cell & Environment **30,** 1107–1125.

Barcelos e Ramos J, Biswas H, Schulz KG, LaRoche J, Riebesell U. 2007. Effect of rising atmospheric carbon dioxide on the marine nitrogen fixer *Trichodesmium*. Global Biogeochemical Cycles **21,** GB2028.

Berman-Frank I, Lundgren P, Chen YB, Küpper H, Kolber Z, Bergman B, Falkowski P. 2001. Segregation of nitrogen fixation and oxygenic photosynthesis in the marine cyanobacterium *Trichodesmium*. Science **294,** 1534–1537.

Boatman TG, Lawson T, Geider RJ. 2017. A key marine diazotroph in a changing ocean: the interacting effects of temperature, CO_2 and light on the growth of *Trichodesmium erythraeum*IMS101. PLoS One **12,** e0168796.

Boatman TG, Mangan NM, Lawson T, Geider RJ. 2018*a*. Inorganic carbon and pH dependency of photosynthetic rates in *Trichodesmium*. Journal of Experimental Botany **69,** 3651–3660.

Boatman TG, Oxborough K, Gledhill M, Lawson T, Geider RJ. 2018*b*. An integrated response of *Trichodesmium erythraeum* IMS101 growth and photo-physiology to iron, CO_2, and light intensity. Frontiers in Microbiology **9,** 624.

Böhme H. 1998. Regulation of nitrogen fixation in heterocyst-forming cyanobacteria. Trends in Plant Science **3,** 346–351.

Buick R. 2008. When did oxygenic photosynthesis evolve? Philosophical Transactions of the Royal Society B: Biological Sciences **363,** 2731–2743.

Campbell L, Carpenter E, Montoya J, Kustka A, Capone D. 2005. Picoplankton community structure within and outside a *Trichodesmium* bloom in the southwestern Pacific Ocean. Vie et Milieu **55,** 185–195.

Capone DG. 2005. Nitrogen fixation by *Trichodesmium* spp.: an important source of new nitrogen to the tropical and subtropical North Atlantic Ocean. Global Biogeochemical Cycles **19**, GB2024.

Capone DG, Zehr JP, Paerl HW, Bergman B, Carpenter EJ. 1997. *Trichodesmium*, a globally significant marine cyanobacterium. Science **276,** 1221–1229.

Carpenter EJ, Capone DG. 1992. Nitrogen fixation in *Trichodesmium* blooms. In: Carpenter EJ, Capone DG, eds. Marine pelagic cyanobacteria: *Trichodesmium* and other diazotrophs. Dordrecht: Kluwer Academic Publishers, 211–217.

Chen YB, Zehr JP, Mellon M. 1996. Growth and nitrogen fixation of the diazotrophic filamentous nonheterocystous cyanobacterium *Trichodesmium* Sp. IMS 101 in defined media: evidence for a circadian rhythm. Journal of Phycology **32,** 916–923.

Collos Y, Mornet F, Sciandra A, Waser N, Larson A, Harrison P. 1999. An optical method for the rapid measurement of micromolar concentrations of nitrate in marine phytoplankton cultures. Journal of Applied Phycology **11,** 179–184.

Davis CS, McGillicuddy DJ Jr. 2006. Transatlantic abundance of the N2-fixing colonial cyanobacterium *Trichodesmium*. Science **312,** 1517–1520.

Eichner MJ, Klawonn I, Wilson ST, Littmann S, Whitehouse MJ, Church MJ, Kuypers MM, Karl DM, Ploug H. 2017. Chemical microenvironments and single-cell carbon and nitrogen uptake in field-collected colonies of *Trichodesmium* under different pCO_2. ISME Journal **11,** 1305–1317.

Eichner M, Kranz SA, Rost B. 2014. Combined effects of different CO_2 levels and N sources on the diazotrophic cyanobacterium *Trichodesmium*. Physiologia Plantarum **152,** 316–330.

Finzi-Hart JA, Pett-Ridge J, Weber PK, Popa R, Fallon SJ, Gunderson T, Hutcheon ID, Nealson KH, Capone DG. 2009. Fixation and fate of C and N in the cyanobacterium *Trichodesmium* using nanometer-scale secondary ion mass spectrometry. Proceedings of the National Academy of Sciences, USA **106,** 6345–6350.

Fu FX, Warner ME, Zhang Y, Feng Y, Hutchins DA. 2007. Effects of increased temperature and CO_2 on photosynthesis, growth and elemental ratios of marine *Synechococcus* and *Prochlorococcus* (Cyanobacteria). Journal of Phycology **43,** 485–496.

Garcia NS, Fu FX, Breene CL, Bernhardt PW, Mulholland MR, Sohm JA, Hutchins DA. 2011. Interactive effects of irradiance and CO_2 on CO_2 fixation and N_2 fixation in the diazotroph *Trichodesmium erythraeum* (Cyanobacteria). Journal of Phycology **47,** 1292–1303.

Geider RJ, Osborne BA. 1989. Respiration and microalgal growth: a review of the quantitative relationship between dark respiration and growth. New Phytologist **112,** 327–341.

Gruber N, Sarmiento JL. 1997. Global patterns of marine nitrogen fixation and denitrification. Global Biogeochemical Cycles **11,** 235–266.

Hutchins DA, Fu F-X, Webb EA, Walworth N, Tagliabue A. 2013. Taxon-specific response of marine nitrogen fixers to elevated carbon dioxide concentrations. Nature Geoscience **6,** 790–795.

Hutchins D, Fu FX, Zhang Y, Warner M, Feng Y, Portune K, Bernhardt P, Mulholland M. 2007. CO_2 control of *Trichodesmium* N_2 fixation, photosynthesis, growth rates, and elemental ratios: implications for past, present, and future ocean biogeochemistry. Limnology and Oceanography **52,** 1293–1304.

Hutchins DA, Walworth NG, Webb EA, Saito MA, Moran D, McIlvin MR, Gale J, Fu FX. 2015. Irreversibly increased nitrogen fixation in *Trichodesmium* experimentally adapted to elevated carbon dioxide. Nature Communications **6,** 8155.

Kana TM. 1992. Relationship between photosynthetic oxygen cycling and carbon assimilation in *Synechococcus* WH7803 (Cyanophyta). Journal of Phycology **28,** 304–308.

Kana TM. 1993. Rapid oxygen cycling in *Trichodesmium thiebautii*. Limnology and Oceanography **38,** 18–24.

Kaplan A, Reinhold L. 1999. CO_2 concentrating mechanisms in photosynthetic microorganisms. Annual Review of Plant Physiology and Plant Molecular Biology **50,** 539–570.

Karl D, Michaels A, Bergman B, Capone D, Carpenter E, Letelier R, Lipschultz F, Paerl H, Sigman D, Stal L. 2002. Dinitrogen fixation in the world's oceans. Biogeochemistry **57,** 47–98.

Kranz SA, Eichner M, Rost B. 2011. Interactions between CCM and N_2 fixation in *Trichodesmium*. Photosynthesis Research **109,** 73–84.

Kranz SA, Levitan O, Richter KU, Prásil O, Berman-Frank I, Rost B. 2010. Combined effects of CO_2 and light on the N_2-fixing cyanobacterium *Trichodesmium* MS101: physiological responses. Plant Physiology **154,** 334–345.

Kranz SA, Sültemeyer D, Richter KU, Rost B. 2009. Carbon acquisition in *Trichodesmium*: the effect of pCO2 and diurnal changes. Limnology and Oceanography **54,** 548–559.

Levitan O, Brown CM, Sudhaus S, Campbell D, LaRoche J, Berman-Frank I. 2010*a*. Regulation of nitrogen metabolism in the marine diazotroph *Trichodesmium* IMS101 under varying temperatures and atmospheric CO_2 concentrations. Environmental Microbiology **12,** 1899–1912.

Levitan O, Rosenberg G, Setlik I, Setlikova E, Grigel J, Klepetar J, Prasil O, Berman-Frank I. 2007. Elevated CO_2 enhances nitrogen fixation and growth in the marine cyanobacterium *Trichodesmium*. Global Change Biology **13,** 531–538.

Levitan O, Sudhaus S, LaRoche J, Berman-Frank I. 2010*b*. The influence of pCO2 and temperature on gene expression of carbon and nitrogen pathways in *Trichodesmium* IMS101. PLoS One **5,** e15104.

Matthijs H, Lubberding H. 1988. Dark respiration in cyanobacteria. In: **Rogers LJ, Gallon JR**, eds. Biochemistry of the algae and cyanobacteria. Proceedings of the Phytochemical Society of Europe. Oxford/New York: Clarendon Press, 131–145.

McGillicuddy DJ. 2014. Do *Trichodesmium* spp. populations in the North Atlantic export most of the nitrogen they fix? Global Biogeochemical Cycles **28,** 103–114.

McKew BA, Davey P, Finch SJ, Hopkins J, Lefebvre SC, Metodiev MV, Oxborough K, Raines CA, Lawson T, Geider RJ. 2013. The trade-off between the light-harvesting and photoprotective functions of fucoxanthin–chlorophyll proteins dominates light acclimation in *Emiliania huxleyi* (clone CCMP 1516). New Phytologist **200,** 74–85.

Miller AG, Espie GS, Canvin DT. 1988. Active transport of inorganic carbon increases the rate of O_2 photoreduction by the cyanobacterium *Synechococcus* UTEX 625. Plant Physiology **88,** 6–9.

Mulholland MR, Bronk DA, Capone DG. 2004. Dinitrogen fixation and release of ammonium and dissolved organic nitrogen by *Trichodesmium* IMS101. Aquatic Microbial Ecology **37,** 85–94.

Nagarajan A, Pakrasi HB. 2001. Membrane-bound protein complexes for photosynthesis and respiration in Cyanobacteria. eLS 1–8.

Platt T, Jassby AD. 1976. The relationship between photosynthesis and light for natural assemblages of coastal marine phytoplankton. Journal of Phycology **12,** 421–430.

Price GD, Badger MR, Woodger FJ, Long BM. 2008. Advances in understanding the cyanobacterial CO_2-concentrating-mechanism (CCM): functional components, Ci transporters, diversity, genetic regulation and prospects for engineering into plants. Journal of Experimental Botany **59,** 1441–1461.

Radmer RJ, Kok B. 1976. Photoreduction of O_2 primes and replaces CO_2 assimilation. Plant Physiology **58,** 336–340.

Raven JA, Beardall J, Giordano M. 2014. Energy costs of carbon dioxide concentrating mechanisms in aquatic organisms. Photosynthesis Research **121,** 111–124.

Raven J, Caldeira K, Elderfield H, Hoegh-Guldberg O, Liss P, Riebesell U, Shepherd J, Turley C, Watson A. 2005. Ocean acidification due to increasing atmospheric carbon dioxide. London: The Royal Society.

Raven J, Falkowski P. 1999. Oceanic sinks for atmospheric CO_2. Plant, Cell & Environment **22,** 741–755.

Ritchie R. 2008. Universal chlorophyll equations for estimating chlorophylls a, b, c, and d and total chlorophylls in natural assemblages of photosynthetic organisms using acetone, methanol, or ethanol solvents. Photosynthetica **46,** 115–126.

Sabine CL, Feely RA, Gruber N, *et al.*.2004. The oceanic sink for anthropogenic CO_2. Science **305,** 367–371.

Schwarz R, Reinhold L, Kaplan A. 1995. Low activation state of ribulose-1,5-bisphosphate carboxylase/oxygenase in carboxysome-defective *Synechococcus* mutants. Plant Physiology **108,** 183–190.

Solorzano L. 1969. Determination of ammonia in natural waters by the phenol hypochlorite method. Limnology and Oceanography **14,** 799–801.

Spungin D, Berman-Frank I, Levitan O. 2014. *Trichodesmium*'s strategies to alleviate phosphorus limitation in the future acidified oceans. Environmental Microbiology **16,** 1935–1947.

Walworth NG, Fu FX, Webb EA, Saito MA, Moran D, McIlvin MR, Lee MD, Hutchins DA. 2016. Mechanisms of increased *Trichodesmium* fitness under iron and phosphorus co-limitation in the present and future ocean. Nature communications **7,** 12081.

Wolk CP. 1968. Movement of carbon from vegetative cells to heterocysts in *Anabaena cylindrica*. Journal of Bacteriology **96,** 2138–2143.

Zeebe RE, Wolf-Gladrow DA. 2001. CO_2 in seawater: equilibrium, kinetics, isotopes. Amsterdam: Elsevier Science.

Zeebe RE, Wolf-Gladrow D, Jansen H. 1999. On the time required to establish chemical and isotopic equilibrium in the carbon dioxide system in seawater. Marine Chemistry **65,** 135–153.